Journal of Molecular Structure 1042 (2013) 78–85

Contents lists available at SciVerse ScienceDirect

Journal of Molecular Structure

journal homepage: www.elsevier.com/locate/molstruc

Synthesis, crystal structure, property research, and DFT calculation of 2,3-diphenylfuro[3,2-*b*]quinoxaline

Qi-Chao Yao, Ding-Er Wu, Min Xia *

Department of Chemistry, Zhejiang Sci-Tech University, Hangzhou 310018, China

HIGHLIGHTS

- Synthesis and X-ray structure of 2,3-diphenylfuro[3,2-*b*]quinoxaline.
- Intense solid-state fluorescence caused by the unique "herring bone" arrangement of the isolated dimers.
- Outstanding electron-accepting ability with the low LUMO level.
- The nature of the large Stokes shift and the positive solvatochromism revealed by DFT calculations.

GRAPHICAL ABSTRACT

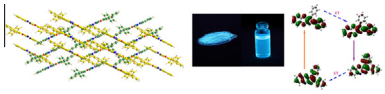

ARTICLE INFO

Article history:
Received 8 February 2013
Received in revised form 25 March 2013
Accepted 25 March 2013
Available online 1 April 2013

Keywords:
2,3-Diphenylfuro[3,2-*b*]quinoxaline
Solid-state fluorescence
Positive solvatochromism
Herring-bone arrangement
Intramolecular charge transfer

ABSTRACT

The title compound is obtained via the intramolecular condensation of 3-(2-oxo-1,2-diphenylethyl)quinoxalin-2(1H)-one in the presence of excessive boron trifluoride etherate and characterized by ^{1}H NMR, ^{13}C NMR, IR, and EI-MS. The solution-based and solid-state fluorescence along with the electrochemical property are studied in detail. The unique herring-bone arrangement which is revealed by the X-ray crystallography should account for the intense solid-state fluorescence. The theoretic calculations are employed to clarify the origin of the large Stokes shift and the positive solvatochromism in view of the geometric relaxation and the transition feature.

1. Introduction

Functional molecules with fluorophores are very important in the fields of chemistry, materials and biology. Molecules exhibiting intense fluorescence both in organic solutions and in solid state have multiple uses. In aspect of the solution fluorescence, they can be utilized as biolabels [1], chemosensors [2], bioprobes [3], detectors in photodynamic therapy [4–6], etc. Although the most common use of solid-state luminescence emitters involves in the area of organic electroluminescence devices (OLEDs) [7,8], other technologies such as solid-state dye lasers [9–11], light-emitting field-effect transistors [12,13], and fluorescent solid sensors [14–16] are also very significant.

Organoboron complexes are one of the most widely used fluorophores due to their distinguishingly photophysical properties [17–19]. We reported the synthesis and property research on a novel type of N,O-bidentate BF_2 complexes with 3-(2-oxo-2-arylethyl)quinoxalin-2(1H)-ones as the ligands [20]. These complexes exhibited the intense green fluorescence in organic solvents along with the outstandingly chemical and photochemical stability. However, these BF_2 complexes were faintly emissive in solid state.

Generally, the introduction of bulky vicinal groups on or close to fluorophores is one of the most effective methods to strengthen the solid-state emission [21–23], as such molecules cannot be tightly stacked due to the space hindrance. Therefore, the notorious concentration-quenching effect [24–26] which is caused by the electronic interactions among molecules can be largely eliminated. Moreover, a considerable geometric relaxation which accounts

* Corresponding author. Tel./fax: +86 571 86843757.
E-mail address: xiamin@zstu.edu.cn (M. Xia).

0022-2860/$ - see front matter © 2013 Elsevier B.V. All rights reserved.
http://dx.doi.org/10.1016/j.molstruc.2013.03.044

for a large Stokes shift usually occurs when a molecule with vicinal groups is excited [27–29].

According to the above concept of molecule design, we intended to prepare the BF_2 complex with 3-(2-oxo-1,2-diphenylethyl)quinoxalin-2(1H)-one as the ligand, wishing it would have the improved solid-state emission. However, it was found that the expected complex was unable to be generated. Instead, 2,3-diphenylfuro[3,2-*b*]quinoxaline was obtained in excellent yield under the same reaction conditions.

Quinoxalines are of great interest because some natural products bearing such skeletons exhibit high biological activities, e.g., echinomycin [30–32], triostin series [33–35], quinoxapeptin series [36,37] and so on. Moreover, conjugated quinoxalines are also very important by virtue of their wide applications as fluorescent probes [38], sensitized dyes in solar cell [39], chelating ligands for metal ions [40], antimicrobial [41], anti-inflammatory [42], antihistaminic [43] agents, Lck enzyme inhibitors [44], etc. For 2,3-diphenylfuro[3,2-*b*]-quinoxaline, where the two vicinal phenyls are imposed on the rigid furo quinoxaline fluorophore, it exhibits the intense solution-based and solid-state fluorescence as well as the large Stoke shift and the positive solvent effect. To our best knowledge, there has no report on the preparation and the property research of this compound.

Herein, we describe the synthesis along with the study on the optical and electrochemical behaviors of this compound. The X-ray crystallography reveals that the intense solid-state fluorescence can be attributed to the unique pattern of molecular stacking. In aid of the theoretic calculations, the insight of the reasons for the large Stokes shift and the positive solvent effect can be afforded.

2. Results and discussion

2.1. Synthesis

The preparation of 2,3-diphenylfuro[3,2-*b*]-quinoxaline can be achieved through a two-step route (Scheme 1), in which *o*-phenylenediamine is initially treated with ethyl 2,4-dioxo-3,4-diphenylbutanoate and the resulting mixture was refluxed in dioxane overnight. Subsequently, the formed intermediate 3-(2-oxo-1,2-diphenylethyl)quinoxalin-2(1H)-one **1** is converted into the titled compound **2** in the presence of triethylamine and boron trifluoride etherate. It is noted that a BF_2 complex will be generated under the same conditions when ethyl 2,4-dioxo-4-phenylbutanoate is utilized as the starting substrate [20].

2.2. Crystal structure

Molecular structure of compound **2** is depicted in Fig. 1a. The detailed crystallographic data and the selected geometric data are listed in Tables 1 and 2 and , respectively. It is shown that the furo[3,2-*b*]quinoxaline core is entirely planar since the torsion angles among C_1–C_6, C_5–N_1 and C_7–O_1 rings are less than 3°. However, the torsion angles between the furyl ring and the two phenyls are 11.68° and 56.96°, respectively. Hence, the C(10)–C(11) bond length was slightly shorter than C(9)–C(17) bond length due to the different extent of coplanarity. Owning to the large space hindrance between the two vicinal phenyls, the aggregated molecules cannot be stacked tightly in their solid state.

It is found that the molecules of compound **2** form the head-to-tail pairs in the crystalline state, these pairs are arranged in a "herring-bone" pattern with a 127.5° tilt angle. Fig. 1b shows that the A–B pair is restrained by the strong π–π interactions whose interplane and centroid distances are 3.432(2) Å and 3.680(2) Å, respectively. The minute difference between these two distances demonstrates that there is a considerable overlapping between the two molecules in this pair. Therefore, a dimer can be generated between molecules A and B. The top view of the dimer A–B is presented in Fig. 1c. The case is the same for molecules E and F. Although the interplane distance of the B–C pair is 3.621(2) Å, the centroid distance of it is 4.467(2) Å. Such a striking difference indicates that the π–π interactions are not sufficiently efficient in this pair, so that a dimer cannot be formed between molecule B and C. The top view of the B–C pair is shown in Fig. 1d. The case is the same for the D–E pair. Importantly, a given dimer barely has the strong interactions with the adjacent dimers. This isolated dimer-type stacking effectively separates molecules from forming the densely electronic interactions with each other [45]. Hence, the considerably raised solid-state fluorescence can be achieved.

2.3. Solution and solid-state photophysical properties

Due to the excellent planarity of the furo[3,2-*b*]-quinoxaline core and the isolated dimer-type stacking of molecules, compound **2** exhibits the very intense blue fluorescence not only in the organic solutions but also in the solid state. The absorption and emission spectra both in CH_3CN and in the solid state are shown in Fig. 2.

In the CH_3CN solution, the λ_{max} for absorption is at 371 nm and the λ_{max} for emission is at 456 nm, respectively. The large Stokes shift (85 nm) can efficiently avoid the occurrence of the self-absorption phenomena, and an improved quantum yield can be offered. Actually, the quantum yield of compound **2** is 0.86 with quinine sulfate as the standard reference. The little overlap of the absorption and fluorescence spectra suggests that a large structural change [46] or charge redistribution [47] takes place in the excited state. Moreover, the molar extinction coefficient ($\varepsilon = 2.77 \times 10^4$ - M^{-1} cm^{-1}) is in agreement with the π–π* transition.

Photos of compound **2** in the CH_3CN solution and in the solid state under a handheld ultraviolet lamp at 365 nm are presented in Fig. 3.

The solvent effect is also investigated, and the resulting spectra are shown in Fig. 4. For the absorption spectra, the maxima are slightly sensitive to the variation of solvent polarity. For the emission spectra, however, the maxima obviously have a bathochromic shift as the solvent polarity increases. This remarkably positive solvatochromism indicates that an intramolecular charge transfer (ICT) occurs in the excited state [48–51]. In a protic solvent such as methanol, compound **2** displays a larger red-shift emission maximum than those in other surveyed solvents. This may well be related to the hydrogen-bond interaction between the excited state and the solvent [52].

In the solid state, compound **2** also displays the intense blue fluorescence, and an image taken under an ultraviolet lamp at 365 nm is shown in Fig. 3. A fairly strong absorption band appears and it becomes much broader than in solutions due to the molecular aggregation. As shown in Fig. 2, however, the emission band centered at 470 nm is extraordinarily sharp. Compared with 77 nm in the CH_3CN solution, the full width at half maximum

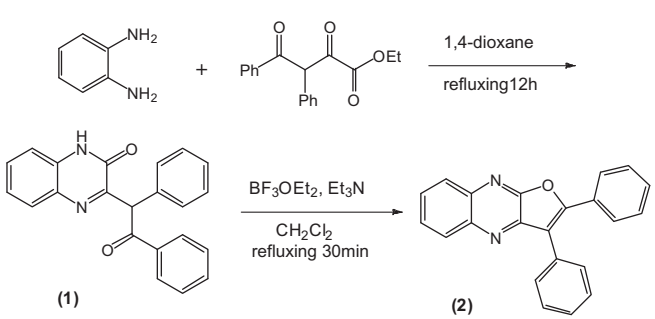

Scheme 1. Route to 2,3-diphenylfuro[3,2-*b*]-quinoxaline.

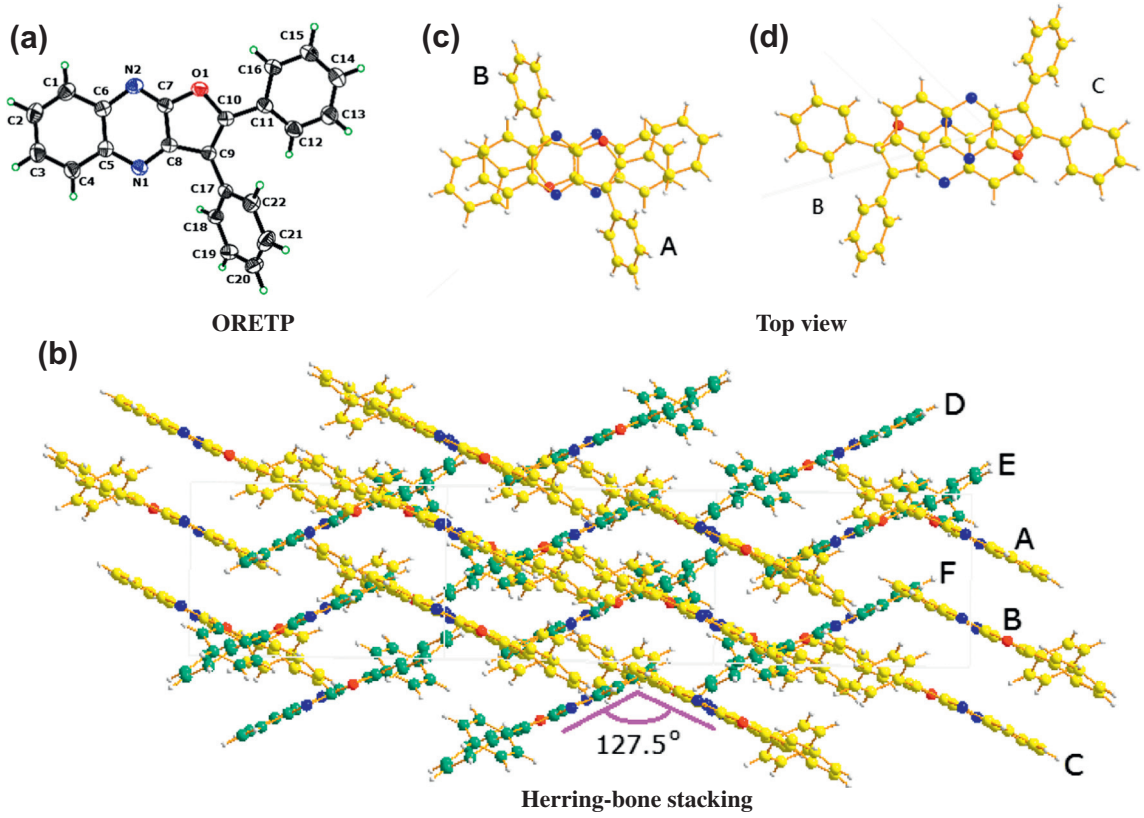

Fig. 1. X-ray crystallography of compound **2**.

Table 1
Crystallographic data and structure refinement details for compound **2.**

Parameter	Data	Parameter	Data
Formula	C_{22} H_{14} N_2O	V/Å^3	3193.57(10)
Formula weight	322.35	Z	8
T/K	298(2)	D_c/g cm^{-3}	1.341
Crystal system	Monoclinic	μ/m m^{-1}	0.084
Space group	C2/c	F(000)	1344
a/Å	23.8787(3)	Crystal size	0.28°0.29°0.38
b/Å	7.8477(4)	θ range	3.24–29.54
c/Å	20.1546(4)	No. of data collected	8027
α/°	90	Independent Reflection	3822 (R_{int} = 0.0225)
β/°	122.27(19)	Goodness-of-fit on F^2	1.008
γ/°	90	Final R index ($I > 2\sigma(I)$)	R = 0.0491, wR = 0.1126

Table 2
Experimental and calculated data of selected bond length and bond angles for compound **2**.

Bond length	Exp (Å)	Cal (Å)	Bond length	Exp (Å)	Cal (Å)	Bond length	Exp (Å)	Cal (Å)
C(5)–N(1)	1.3743	1.3666	C(8)–N(1)	1.3233	1.3193	C(7)–C(8)	1.4130	1.4309
C(6)–N(2)	1.3768	1.3730	C(7)–N(2)	1.2898	1.2951	C(9)–C(17)	1.4733	1.4773
C(7)–O(1)	1.3584	1.3610	C(10)–O(1)	1.3991	1.3946	C(10)–C(11)	1.4608	1.4629
Bond angle	**Exp (°)**	**Cal (°)**	**Bond angle**	**Exp (°)**	**Cal (°)**	**Bond angle**	**Exp (°)**	**Cal (°)**
C(4)–C(5)–N(1)	118.592	118.942	C(5)–N(1)–C(8)	113.705	114.816	N(1)–C(8)–C(9)	131.341	132.188
C(1)–C(6)–N(2)	118.722	119.037	C(6)–N(2)–C(7)	111.957	113.152	N(2)–C(7)–O(1)	122.634	123.737
C(7)–O(1)–C(10)	106.443	106.825	C(8)–C(9)–C(17)	125.048	125.086	O(1)–C(10)–C(11)	112.913	113.853

Torsion angle	Exp (°)	Cal (°)	Torsion angle	Exp (°)	Cal (°)
C(18)–C(17)–C(9)–C(8)	56.958	51.079	C(16)–C(11)–C(10)–O(1)	12.597	25.148
C(8)–C(9)–C(10)–O(1)	0.449	1.726	C(9)–C(8)–C(7)–N(2)	−177.600	−179.110
C(10)–C(9)–C(8)–N(1)	−179.136	−179.624	C(3)–C(4)–C(5)–N(1)	−178.491	−179.964
O(1)–C(7)-C(8)–N(1)	−179.750	−179.845	C(2)–C(1)–C(6)–N(2)	−179.734	−179.899

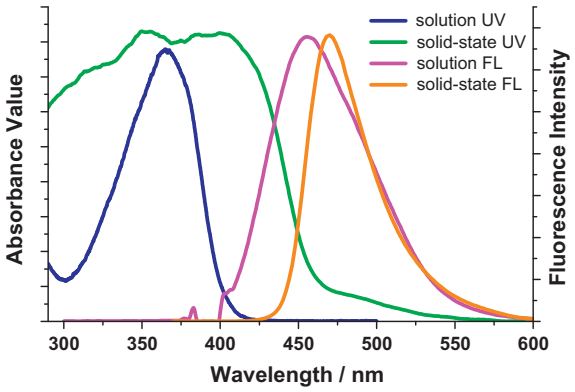

Fig. 2. Normalized UV–Vis absorption and fluorescence spectra of compound **2.**

Fig. 3. Solution and solid-state fluorescence of compound **2** at 365 nm irradiation.

height (FWHM) is only 46 nm in the solid state. The considerably sharpened FWHM suggests that there are only weak interactions among the aggregated molecules in the solid state [53,54].

In our work, the "herring-bone" arrangement of the isolated dimers prevents molecules from forming a network via the π–π stacking, thus the spectral broadening can be effectively avoided. It was reported that [55] the difference between the emission maxima in solutions and in the solid state may be used as an indicator to evaluate the intermolecular π–π interactions. For compound **2,** the value is only 14 nm. Such a relatively small difference implies that a dense network of the π–π interactions hardly exists in the solid state. The measured quantum yield in the solid state is 0.28, which is high enough for a solid-state emitter.

In summary, a limited extent of intermolecular interactions together with the large Stokes shifts is beneficial for the elimination of the self-quenching and the improvement of the solid-state fluorescence.

2.4. Electrochemical feature

It is well known that the HOMO and the LUMO level energy of a given molecule at its ground state can be estimated by the cyclic

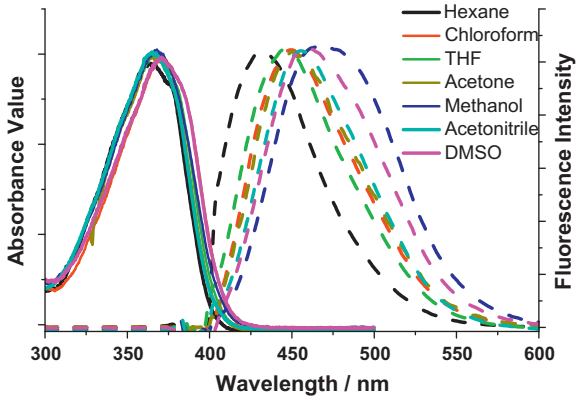

Fig. 4. Normalized spectra of solvent effect on compound **2** (solid lines for absorption and dash lines for emission).

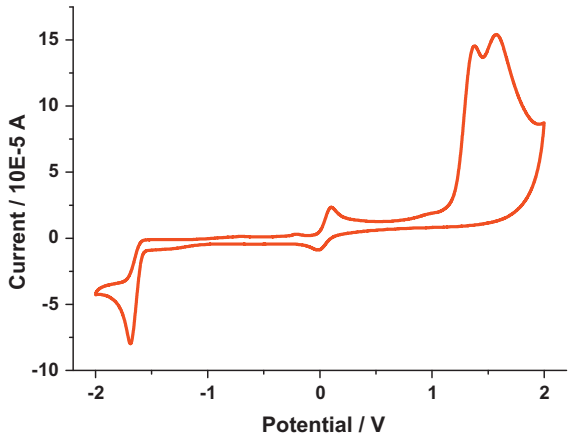

Fig. 5. Cyclic voltammogram of compound **2.**

voltammetry (CV). The measured cyclic voltammogram of compound **2** which is calibrated by the reference to the ferrocene pair in anhydrous acetonitrile [56] is presented in Fig. 5.

It is shown that both the oxidation and the reduction process are irreversible for compound **2.** The oxidative onset potential is 1.21 V and the reductive onset potential is −1.59 V. Therefore, the corresponding ionization potential (IP, HOMO level) is −6.01 eV and the electron affinity (EA, LUMO level) is −3.21 eV. It is found that the optical energy gap (E_g = 3.11 eV), which is calculated on the lowest-energy edge of the UV–Vis absorption spectrum, is very close to the electrochemical energy gap (E_g = 2.80 eV). Such relatively wide energy gap indicates that compound **2** can be used as an efficient bright-violet to blue fluorescence emitter. Compared with the commonly used electron-transport material Alq_3 whose LUMO level is approximately −3.0 eV [57,58], our compound has the lower LUMO level. Hence,

Table 3
Selected electronic transition energies and corresponding oscillator strengths (*f*), main compositions and CI coefficients of the low-lying electronic states of compound **2**.

Electronic transition	TD-DFT-PCM/B3LYP/6-31G++(d,p)			
	Energy (eV)	Oscillator strength (*f*)	Composition	CI coefficient
$S_0 \rightarrow S_1$	3.08 ev (401 nm)	0.4362	H → L	0.6961
$S_0 \rightarrow S_2$	3.68 eV (337 nm)	0.0091	H-5 → L	0.4176
			H-4 → L	0.2625
			H-2 → L	0.2885
			H-1 → L	0.3875
$S_1 \rightarrow S_0$	2.47 eV (502 nm)	0.2622	H → L	0.7001
$S_2 \rightarrow S_0$	3.47 eV (357 nm)	0.0638	H-1 → L	0.6556
			H→L + 1	0.2294

the better electron-accepting capacity of our compound will make it more appealing in practical applications as an electroluminescence material.

2.5. Theoretical calculations

The geometry of compound **2** is optimized in the singlet state using the density functional theory (DFT) method at the B3LYP level, and the 6-31G++(d,p) basis set is chosen. In general, the predicted bond lengths and angles are in good agreement with the values based on the X-ray crystal structure data (see Table 2). The major difference between the experimental and the calculated geometry lies in the C(16)–C(11)–C(10)–O(1) torsion angle. The X-ray-determined angle is 11.679° while the calculated one is 25.148°. Such deviation is derived from the different molecular environments, where the geometric optimization is carried out for isolated molecules in gas phase while the experimental results are based on molecules interacting in the solid state. Consequently, the intermolecular interactions should account for the difference in geometric parameters [59]. The calculated data render a reasonable geometry for the further stimulations.

With the TD-DFT calculations under the polarizable continuum model (PCM), the first absorption and emission maxima in CH_3CN are predicted. The simulated λ_{ab} and λ_{em} are at 401 nm and 502 nm respectively, which are in good agreement with the experimentally measured values at 371 nm and 456 nm. It is indicated in Table 3 that both the first absorption and the emission are dominantly attributed to the transitions between the HOMO and the LUMO, which can be assigned to a π–π^* transition. As shown in Fig. 6, the HOMO is distributed on the entire molecule whereas the LUMO is excluded from the C_{17}–C_{22} ring. Obviously, an intramolecular charge transfer (ICT) occurs in the photo-induced excitation of compound **2**. Hence, an assumed ICT transition which accounts for the positive solvatochromism on the emission spectra is definitely confirmed by the TD-DFT calculations.

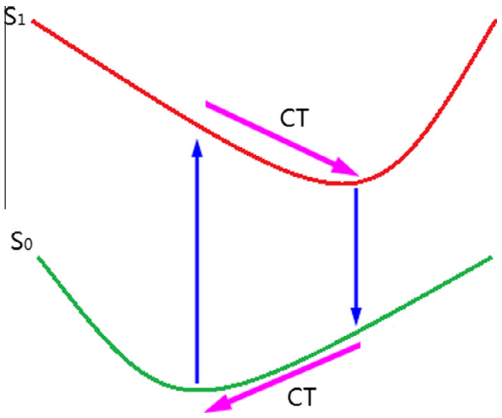

Fig. 7. Simplified Jablonski diagram for the origin of the large Stoke's shifts due to the conformation transformation.

In principle, the Stokes shift is caused by the geometry relaxation at the S_1 state after the vertical excitation from the S_0 state, i.e., from the Franck–Condon excited state to the energy-minimized geometry at the S_1 state [60,61] (Fig. 7). For compound **2**, the DFT calculations under PCM conditions clearly demonstrate (Fig. 8) that a substantial conformation transformation occurs between the S_0 and the S_1 state in CH_3CN, since the torsion angle C(18)–C(17)–C(9)–C(8) is decreased from 51.08° in the S_0 state to 29.91° in the S_1 state. Meanwhile, a tiny decrease of the torsion angle C(16)–C(11)–C(10)–O(1) takes place from the S_0 to the S_1 state. This photo-induced geometric relaxation has a pronounced influence on the energy level of the frontier molecular orbitals. It is found that the LUMO level is stabilized by 0.24 eV in the S_1 state compared with that in the S_0 state, but the HOMO level is destabilized by 0.37 eV in the S_1 state compared with that in the S_0 state. As a result, the energy gap between the HOMO and the LUMO is remarkably reduced from the absorption to the emission

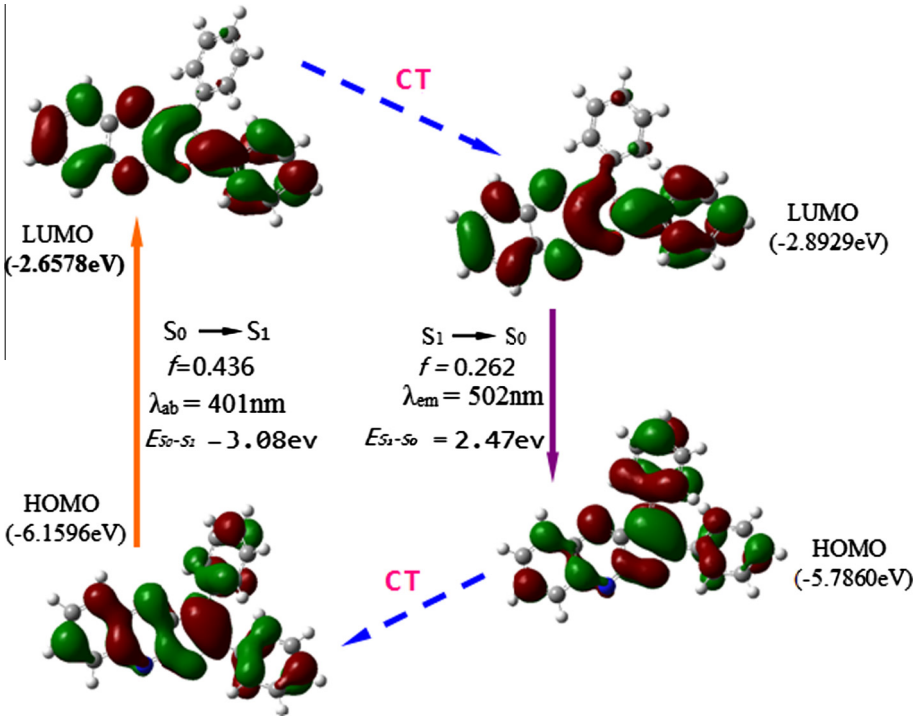

Fig. 6. Rationalization of the UV–Vis absorption, emission and the large Stokes shift of compound **2** in acetonitrile (CT stands for conformation transformation; Calculation with TD-DFT-PCM under B3LYP level at 6-31G++(d,p) basis set).

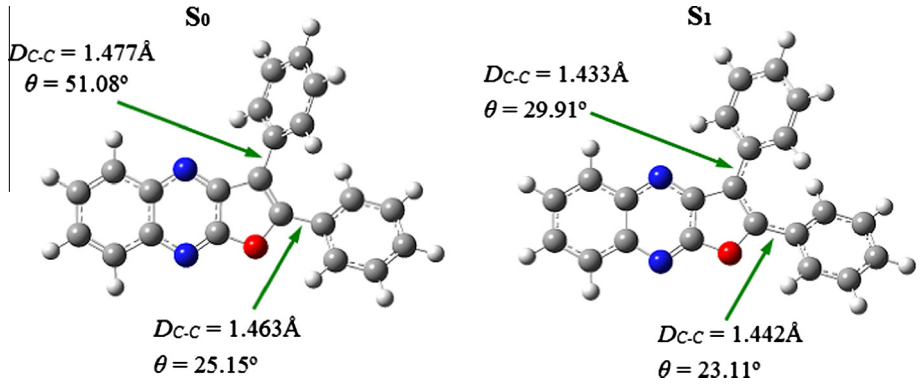

Fig. 8. Geometry of compound **2** at the ground state (S_0) and the first singlet excited state (S_1).

transition. Therefore, it is reasonable to assume that the geometric relaxation between the S_0 and the S_1 state should be responsible for the large Stokes shift of compound **2.**

According to the following Einstein transition probability formula (in au) [62,63]:

$$\tau = \frac{c^3}{2(E_{FL})^2 f}$$

where c is the velocity of light, E_{FL} is the vertical emission energy, and f is the oscillator strength, the calculated radiative lifetime τ of our compound in CH_3CN is 14.47 ns. The relatively long lifetime makes this compound potential as a candidate in many fields involving the applications of fluorescence.

3. Conclusion

Herein we report the synthesis of a novel compound 2,3-diphenylfuro[3,2-*b*]quinoxaline and the research on its photophysical and electrochemical properties. The X-ray crystallography indicates that the unique "herring-bone" arrangement of the isolated dimers, by which the network of the π–π stacking can be dramatically inhibited, is the main reason for the intense solid-state fluorescence. An assumed ICT transition accounting for the solvent-reliant emission is confirmed by the TD-DFT calculations. Additionally, the theoretical simulation reveals that the geometric relaxation from the S_0 to the S_1 state should be responsible for the large Stokes shift. Moreover, the low LUMO level and the long radiative lifetime make this compound as a promising material in fields involving OLEDs, fluorescence imaging, and so on.

4. Experimental

4.1. Materials and measurements

All the reagents were analytically pure and some chemicals were further purified by recrystallization or distillation. Melting points were determined by an X-4 micro-melting instrument and the thermometer was uncorrected. The ^{1}H NMR (400 MHz) and ^{13}C NMR (100 MHz) spectra were obtained on a Bruker Avance II DMX 400 spectrometer with DMSO-d_6 as the solvent. FT-IR spectra were obtained with KBr pellets on a Nicolet Avatar spectrophotometer. The absorption spectra were measured on a Shimadzu UV 2501(PC)S UV–Vis spectrometer, and the fluorescence spectra were acquired on a Perkin–Elmer LS55 spectro-photometer. The quantum yield in CH_3CN was measured with quinine sulfate in 0.1 M sulfuric acid as the reference (Φ_f = 0.55) and the quantum yield in the solid state was gained by an integral sphere. The mass spectrum was recorded on a HP 1110 mass spectrometer. The cyclic voltammogram was obtained on a ChenHua CHI660B electrochemical working station with 2 mM sample in an anhydrous acetonitrile solution of 0.1 M tetrabutylammonium perchlorate, using a carbon glass as the working electrode, a platinum wire as the counting electrode and a 0.01 M Ag/Ag$^+$ pair as the reference electrode. The scan rate was at 30 mV/s and 0.5 mM ferrocene was used as the internal standard. The HOMO and the LUMO levels were obtained by correlating the onsets of Fc/Fc+ pair to the normal hydrogen electrode (NHE), assuming the HOMO level of the Fc/Fc+ to be 4.88 eV. The single crystal structure was determined on a Bruker Gemini Ultra diffractometer with a CCD counter.

4.2. Synthesis

4.2.1. Preparation of 3-(2-oxo-1,2-diphenylethyl)quinoxalin-2(1H)-one (1)

At room temperature, ethyl 2,4-dioxo-3,4-diphenylbutanoate (0.296 g, 1 mmol) was added to the solution of *o*-phenylenediamine (0.108 g, 1 mmol) in 1,4-dioxane (5 mL). The mixture was refluxed for 12 h and the precipitated white solid was collected. The solid was washed with ethanol and ether for several times before being dried under vaccum.

0.278 g (0.82% yield), m.p. 233–235 °C; IR (KBr) ν (cm^{-1}): 3430, 3060, 1666, 1496, 1290, 1212, 752, 696; ^{1}H NMR(400 MHz, DMSO-d_6) δ(ppm): 6.69(s, 1H), 7.26–7.38(m, 5H), 7.45–7.52(m, 5H), 7.59(d, *J* = 8 Hz, 2H), 8.06(d, *J* = 8 Hz, 2H), 12.58(s, 1H); ^{13}C NMR(100 MHz, DMSO-d_6) δ(ppm): 55.91, 115.43, 123.35, 127.27, 128.27, 128.51, 128.64, 128.78, 130.17, 130.44, 131.26, 131.71, 133.21, 134.59, 135.90, 154.07, 159.56, 195.91; EI-MS *m/z* (%): 340(M^+, 20), 235(23), 206(35), 105(100), 91(15), 77(85), 51(18).

4.2.2. Preparation of 2,3-diphenylfuro[3,2-b]-quinoxaline (2)

At room temperature, triethylamine (0.51 g, 5 mmol) was dropped into the suspension of (**1**) (0.68 g, 2 mmol) in CH_2Cl_2 (15 mL) and the resulting mixture was stirred for 20 min. Boron trifluoride etherate (1.42 g, 10 mmol) was then added and the mixture was refluxed for 30 min. After cooling to room temperature, the mixture was diluted with water. The organic layer was separated and dried over anhydrous Na_2SO_4. The filtrate was concentrated and the residue was purified by column chromatography (hexane/ethyl acetate 5:1) to provide compound (**2**) as a yellow powder.

0.30 g (93% yield), m.p. 210–212 °C; IR (KBr) ν (cm^{-1}): 1626, 1405, 1308, 1056, 1033, 953, 757, 693; ^{1}H NMR(400 MHz, DMSO-d_6) δ(ppm): 7.49(t, *J* = 8 Hz, 2H), 7.58–7.65 (m, 6H), 7.93–8.02(m, 4H), 8.33(d, *J* = 8 Hz, 1H), 8.53(d, *J* = 8 Hz, 1H); ^{13}C NMR (100 MHz, DMSO-d_6) δ(ppm): 116.57, 128.04, 128.07, 128.57, 128.58, 128.75, 128.89, 120.09, 129.12, 129.25, 129.81, 129.96,

130.85, 139.07, 142.42, 144.34, 153.63, 158.27; EI-MS *m/z* (%): 322(M^+, 100), 293(17), 176(21), 90(15), 77(28).

4.3. X-ray structure analysis

A single crystal of compound **2** (0.28 mm × 0.29 mm × 0.38 mm) was selected for the X-ray analysis. The diffraction data were collected on a Bruker CCD area-detector diffractometer equipped with a graphite-monochromated Mo Ka radiation (λ = 0.71073 Å) at room temperature (298 K). The unit cell parameters were determined from a least-squares refinement of the setting angles with θ in the range $3.24 \leqslant \theta \leqslant 29.54$. The structure was solved by direct methods and refined on F^2 by the full-matrix least-squares methods with SHELXS-97 [64]. The refinement was carried out by full-matrix least squares method on the positional and anisotropic temperature parameters of the non-hydrogen atoms, or equivalently corresponding to 226 crystallographic parameters, using SHELXL-97 [65]. All H atoms were placed in the idealized positions and constrained to ride on their parent atoms. The molecular graphics were generated using ORTEP-3 [66].

4.4. Computational method

Full geometry optimizations were carried out using the density functional theory (DFT) method at the B3LYP level for compound **2** [67,68]. The 6-31G++(d,p) basis set was used for all the elements. The vibration frequency calculations were performed to ensure that the optimized geometries represent the local minima. All calculations were performed with the Gaussian 09 program package and the GaussView visualization program [69]. The vertical transitions based on the B3LYP optimized geometries were computed using the time-dependent density functional theory (TD-DFT) and the solvent effects were stimulated with the polarizable continuum model (PCM) [70,71].

Supplementary material

CCDC 907558 contains the supplementary crystallographic data for this paper. These data can be obtained free of charge from The Cambridge Crystallographic Data Centre via www.ccdc.cam.ac.uk/data_request/cif.

Acknowledgement

We are grateful for the financial support of the Zhejiang Natural Science Foundation (Y4100034) and Zhejiang Province Key Innovation Team (2012R 10038-09).

References

[1] R.P. Haugland, Handbook of Molecular Probes and Research Products, 9th ed., Molecular Probes, Eugene, 2002.
[2] A.W. Czarnik, Fluorescent Chemosensors for Ion and Molecular Recognition, American Chemical Society, 1993.
[3] R.Y. Tsien, Fluorescent and Photochemical Probes of Dynamic Biochemical Signals Inside Living Cells, American Chemical Society, 1993.
[4] S. Erbas, A. Gorgulu, M. Kocakusakogullari, E.U. Akkaya, Chem. Commun. (2009) 4956–4958.
[5] C.D. Entwistle, T.B. Marder, Chem. Mater. 16 (2004) 4574–4585.
[6] J. Davila, A. Harriman, K.S. Gulliya, Photochem. Photobiol. 53 (1991) 1–11.
[7] A.C. Grimsdale, K.L. Chan, R.E. Martin, P.G. Jokisz, A.B. Holmes, Chem. Rev. 109 (2009) 897–1091.
[8] R.H. Friend, R.W. Gymer, A.B. Holmes, J.H. Burroughes, R.N. Marks, C. Taliani, D.D.C. Bradley, D.A. Dos Santos, J.L. Brédas, M. Lödlund, W.R. Salaneck, Nature 397 (1999) 121–128.
[9] S.C. Lo, P.L. Burn, Chem. Rev. 107 (2007) 1097–1116.
[10] U. Scherf, S. Riechel, U. Lemmer, R.F. Mahrt, Curr. Opin. Solid State Mater. Sci. 5 (2001) 143–154.
[11] G. Kranzelbinder, G. Leising, Rep. Prog. Phys. 63 (2000) 729–762.
[12] J. Zaumseil, H. Sirringhaus, Chem. Rev. 107 (2007) 1296–1323.
[13] F. Cicoira, C. Santato, Adv. Funct. Mater. 17 (2007) 3421–3434.
[14] S.W. Thomas, G.D. Joly, T.M. Swager, Chem. Rev. 107 (2007) 1339–1386.
[15] P. Carol, S. Sreejith, A. Ajayaghosh, Chem. Asian J. 2 (2007) 338–348.
[16] L. Basabe-Desmonts, D.N. Reinhoudt, M. Crego-Calama, Chem. Soc. Rev. 36 (2007) 993–1017.
[17] A.C. Benniston, G. Copley, Phys. Chem. Chem. Phys. 11 (2009) 4124–4131.
[18] R. Ziessel, G. Ulricha, A. Harrimanb, New J. Chem. 31 (2007) 496–501.
[19] G. Ulrich, R. Ziessel, Angew. Chem. Int. Ed. 47 (2008) 1184–1201.
[20] M. Xia, B. Wu, G.F. Xiang, J. Fluorine Chem. 129 (2008) 402–408.
[21] N.J. Turro, Modern Molecular Photochemistry, University Science Books, Mill Valley, 1991.
[22] B. Valeur, Molecular Fluorescence: Principle and Applications, Wiley-VCH, Weinheim, 2002.
[23] K. Shirai, M. Matsuokab, K. Fukunishi, Dye Pig. 42 (1999) 95–101.
[24] Y. Zhou, Y. Xiao, S. Chi, X. Qian, Org. Lett. 10 (2008) 633–636.
[25] H. Zhang, X. Hua, W. Dou, W. Liu, J. Fluorine Chem. 131 (2010) 883–887.
[26] S.-Y. Park, M. Ebihara, Y. Kubota, K. Funabiki, M. Matsui, Dyes Pig. 82 (2009) 258–267.
[27] D. Huang, Y. Chen, J. Zhao, Dyes Pig. 95 (2012) 732–742.
[28] P. Song, S.-G. Sun, J.-Y. Liu, Y.-Q. Xu, K.-L. Han, X.-J. Peng, Spectroscopy 74 (2009) 753–757.
[29] F. Liu, P. Zuo, L. Meng, S.J. Zheng, J. Molecul. Struct. Therochem. 726 (2005) 161–169.
[30] A. Milesi-Hallè, S. Mecullough, J.A. Hinson, R.C. Kurten, L.W. Lamps, A. Brown, L.P. James, Basic Clin. Pharm. Toxic. 110 (2012) 327–334.
[31] Y.S. Park, W.S. Shin, S.K. Kim, J. Antimicrob. Chemother. 61 (2008) 163–168.
[32] M.J. Waring, L.P. Wakelin, Nature 252 (1974) 653–656.
[33] O.E. Zolova, A.S.A. Mady, S. Garneau-Tsodikova, Biopolymers 93 (2009) 777–790.
[34] H. Otsuka, J. Shoji, Tetrahedron 23 (1967) 1535–1542.
[35] M. Bailly, M.J. Waring, Biochem. J. 330 (1998) 81–87.
[36] D.L. Boger, M.W. Ledeboer, M. Kume, M. Searcey, Q. Jin, J. Am. Chem. Soc. 121 (1999) 11375–11383.
[37] R.B. Lingham, A.H.M. Hsu, J.A. O'Brien, J.M. Sigmund, M. Sanchez, M.M. Gagliardi, B.K. Heimbuch, O. Genilloud, I. Martin, M.T. Diez, C.F. Hirsch, D.L. Zink, J.M. Liesch, G.E. Koch, S.E. Gartner, G.M. Garrity, N.N. Tsou, G.M. Salituro, J. Antibiot. 49 (1996) 253–259.
[38] H. Benzeid, E. Mothes, El.M. Essassi, P. Faller, G. Pratriel, Comp. Rend. Chim. 15 (2012) 79–85.
[39] S. Eu, S. Hayashi, T. Umeyama, Y. Matano, Y. Araki, H. Imahori, J. Phys. Chem. C 112 (2008) 4396–4405.
[40] C.J. Sumby, Aust. J. Chem. 61 (2008) 894–904.
[41] A.M. Soliman, A.A. Amer, Synth. Commun. 42 (2012) 1401–1410.
[42] J.T. Leonard, O.S. Rajesh, K. Murugesh, V. Gunasekaran, Asian J. Chem. 17 (2005) 2669–2673.
[43] Ch. Sridevi, A. Balaji, A. Naidu, E. J.Org. Chem. 8 (2011) 924–930.
[44] P. Chen, E.J. Iwanowicz, D. Norris, D.D. Gu, J. Lin, R.V. Moquin, J. Das, J. Wityak, S.H. Spergel, H. Fex, S. Pang, S. Pitt, D.R. Shen, G.L. Schieven, J.C. Barrish, Bioorg. Med. Chem. Lett. 12 (2002) 3153–3156.
[45] S.Y. Park, M. Ebihara, Y. Kubota, K. Funabiki, M. Matsui, Dyes Pig. 82 (2009) 258–267.
[46] M. Shimizu, Y. Asai, Y. Takeda, A. Yamatani, T. Hiyama, Tetrahedron Lett. 52 (2011) 4084–4089.
[47] Z.R. Grabowski, K. Rotkiewicz, W. Rettig, Chem. Rev. 103 (2003) 3899–4031.
[48] D. Huang, Y. Chen, J. Zhao, Dyes Pig. 95 (2012) 732–742.
[49] G.J. Huang, J.H. Ho, C. Prabhakar, Y.H. Liu, S.M. Peng, J.S. Yang, Org. Lett. 14 (2012) 5034–5037.
[50] B. Wang, H. Liao, H. Yeh, W. Wu, C. Chen, J. Lumin. 113 (2005) 321–328.
[51] C. Cornelissen-Gude, W. Rettig, J. Phys. Chem. A 103 (1999) 4371–4377.
[52] Z.R. Grabowski, K. Rotkiewicz, Chem. Rev. 103 (2003) 3899–4032.
[53] K.-C. Wu, P.-J. Ku, C.-S. Lin, H.-T. Shih, F.-I. Wu, M.-J. Huang, J.-J. Lin, I.-C. Chen, C.-H. Cheng, Adv. Funct. Mater. 18 (2008) 67–75.
[54] H. Tong, Y. Dong, Y. Hong, M. Haeussler, J.W.Y. Lam, H.H.Y. Sung, X. Yu, J. Sun, I.D. Williams, H.S. Kwok, B.Z. Tang, J. Phys. Chem. C 111 (2007) 2287–2294.
[55] K. Shirai, M. Matsuokab, K. Fukunishi, Dyes Pig. 42 (1999) 95–101.
[56] V.V. Pavlishchuk, A.W. Addison, Inorg. Chim. Acta 298 (2000) 97–102.
[57] P.E. Burrows, Z. Shen, V. Bulovic, D.M. McCarty, S.R. Forrest, J.A. Cronin, M.E. Thompson, J. Appl. Phys. 79 (1996) 7991–8006.
[58] J. Shinar, Organic Light-Emitting Devices: a Survey, Springer-Verlag, New York, Inc., New York, 2003.
[59] H. Tanak, Y. Kösal, Struct. Chem. 20 (2009) 409–416.
[60] N.J. Turro, V. Ramamurthy, J.C. Scaiano, Principles of Molecular Photochemistry: An Introduction, University Science Books, Sausalito, 2009.
[61] Y. Chen, J. Zhao, H. Guo, L. Xie, J. Org. Chem. 77 (2012) 2192–2206.
[62] M.E. Casida, C. Jamorski, K.C. Casida, D.R. Salahub, J. Chem. Phys. 108 (1998) 4439–4449.
[63] V. Lukeš, A. Aquino, H. Lischka, J. Phys. Chem. A 109 (2005) 10232–10238.
[64] G.M. Sheldrick, SHELXS-97, Program for Crystal Structure Solution, University of Göttingen, Germany, 1997.
[65] G.M. Sheldrick, SHELXL-97, Program for Crystal Structure Refinement, University of Göttingen, Germany, 1997.
[66] L.J. Farrugia, J. Appl. Crystallogr. 30 (1999) 837–838.
[67] A.D. Becke, J. Chem. Phys. 98 (1993) 5648–5652.
[68] C. Lee, W. Yang, R.G. Parr, Phys. Rev. B 37 (1988) 785–789.
[69] M.J. Frisch, G.W. Trucks, H.B. Schlegel, G.E. Scuseria, M.A. Robb, J.R. Cheeseman, G. Scalmani, V. Barone, B. Mennucci, G.A. Petersson, H. Nakatsuji, M. Caricato,

X. Li, H.P. Hratchian, A.F. Izmaylov, J. Bloino, G. Zheng, J.L. Sonnenberg, M. Hada, M. Ehara, K. Toyota, R. Fukuda, J. Hasegawa, M. Ishida, T. Nakajima, Y. Honda, O. Kitao, H. Nakai, T. Vreven, J.A. Montgomery, Jr., J.E. Peralta, F. Ogliaro, M. Bearpark, J.J. Heyd, E. Brothers, K.N. Kudin, V.N. Staroverov, T. Keith, R. Kobayashi, J. Normand, K. Raghavachari, A. Rendell, J.C. Burant, S.S. Iyengar, J. Tomasi, M. Cossi, N. Rega, J.M. Millam, M. Klene, J.E. Knox, J.B. Cross, V. Bakken, C. Adamo, J. Jaramillo, R. Gomperts, R.E. Stratmann, O. Yazyev, A.J. Austin, R. Cammi, C. Pomelli, J.W. Ochterski, R.L. Martin, K. Morokuma, V.G. Zakrzewski, G.A. Voth, P. Salvador, J.J. Dannenberg, S. Dapprich, A.D. Daniels, O. Farkas, J.B. Foresman, J.V. Ortiz, J. Cioslowski, D.J. Fox, Gaussian 09, Revision B.01, Gaussian, Inc., Wallingford CT, 2010.

[70] M. Cossi, N. Rega, G. Scalmani, V. Barone, J. Comput. Chem. 24 (2003) 669–681.

[71] N.M. O'Boyle, A.L. Tenderholt, K.M. Langner, J. Comput. Chem. 29 (2008) 839–845.